Ripple Rotation in Multilayer Homoepitaxy

F. Buatier de Mongeot, G. Costantini, C. Boragno, and U. Valbusa

INFM-Unità di Ricerca di Genova, Centro CFSBT-CNR and Dipartimento di Fisica, Via Dodecaneso 33, I-16146 Genova, Italy

(Received 5 November 1999)

We have investigated the homoepitaxial growth of Ag(110) in the multilayer regime. After deposition of 30 monolayers of Ag at a temperature of 210 K a ripplelike surface instability is produced and the ridges of the ripples, as well as the majority steps, are found to be parallel to $\langle 1\bar{1}0\rangle$ which is the thermodynamically favored orientation. As the deposition temperature is decreased to 130 K, an unexpected 90° switch of the ripple orientation is observed. The ridges of the ripples and the steps are in this case parallel to $\langle 100\rangle$. In the intermediate temperature range a checkerboard of rectangular mounds results. We interpret our results in terms of the peculiar hierarchy of interlayer and intralayer diffusion barriers present on the anisotropic Ag(110) surface.

PACS numbers: 68.55.–a, 61.14.Hg, 68.35.Fx, 68.65.+g

Homoepitaxial growth on single crystal surfaces has attracted much attention, being the simplest possible test bench for understanding the technological relevant process of thin film growth. In the case of both semiconductors and metals, the deposition of several tens of monolayers has been reported to produce progressing kinetical roughening of high symmetry surfaces, accompanied by the growth of three-dimensional mounds. In the case of single crystal metal surfaces with equivalent diffusion [e.g., (001) or (111) terminations of fcc crystals], these mounds are characterized by regular shapes and pattern the surface in a periodical fashion depending on the substrate symmetry: square pyramidlike mounds were reported in the case of Cu on Cu(001) [1] and Fe on Fe(001) [2,3], hexagonal ones for Pt on Pt(111) [4]. The evolution of this type of self-assembled nanostructures is enhanced whenever the diffusing adatoms experience an extra energy barrier at the step edges (the so-called Ehrlich-Schwoebel (ES) barrier [5,6]). In this case, the probability that an adatom bounces back at a step edge is higher than the probability that it descends to the lower terrace, and thus a net adatom uphill current is established in the direction perpendicular to the steps. Such a current enhances the nucleation of islands on the upper terrace and the iteration of this process leads to formation of mounds, as also demonstrated by discrete computer simulations [7,8]. The usual theoretical approach to this type of growth phenomena is represented by a continuum model [9], in which the local surface height h obeys the conservation law

$$\partial_t h(\mathbf{r}, t) = -\nabla \cdot \mathbf{j}(\mathbf{r}, t) + \eta(\mathbf{r}, t). \qquad (1)$$

Here η is a shot noise function that accounts for the spatial and temporal randomness of the adatom arrivals and $\mathbf{j}$ is the total surface current given by the sum of a destabilizing contribution $\mathbf{j}_s$ (the above described adatom uphill caused by the ES barrier) and a stabilizing term $\mathbf{j}_{\mathrm{eq}}$ which accounts for the smoothing effect of adatom diffusion. According to Refs. [10,11], for an isotropic surface characterized by local slopes smaller than 1, the uphill current $\mathbf{j}_s$ can be written as

$$\mathbf{j}_s(\mathbf{m}) \propto \mathbf{m}/[1 + (l_d \mathbf{m})^2], \qquad (2)$$

where l_d is the diffusion length, i.e., the average distance that an adatom can travel on the surface before it incorporates into islands or steps and $\mathbf{m} = \nabla h$ is the vector describing the local surface slope. The integration of Eq. (1) using the uphill current [Eq. (2)] results in a surface morphology characterized by the experimentally observed moundlike features [10,11].

Most of the theoretical work done until now has dealt with only isotropic surfaces. Siegert and Plischke actually considered the effects of a crystalline substrate, but only in the case of surfaces endowed with cubic symmetry which are still isotropic in the sense that their principal crystallographic directions are equivalent [11]. On the other hand, anisotropic substrates have different values of the diffusion energy barriers along the nonequivalent crystallographic directions, and may thus be characterized by uphill currents which depend on the surface direction. The class of (110) terminated bcc metals has been experimentally studied, for instance in the case of Fe homoepitaxy on Fe(110) [12], concluding that elongated mounds develop with ridges aligned along $\langle 100\rangle$ in the whole range of investigated temperatures. More interesting is the case of (110) terminated fcc metal substrates since two orthogonal diffusion directions exist, the "easy" in-channel $\langle 1\bar{1}0\rangle$ and the "hard" cross-channel $\langle 100\rangle$ [13]. Moreover, nonequivalent ES barriers are present at the steps along $\langle 100\rangle$ and $\langle 1\bar{1}0\rangle$. In this case the surface temperature establishes a hierarchy for the activation of the relevant diffusion processes, and it should be possible to determine the direction of the current by simply acting on the temperature during deposition. In order to check the correctness of this guess, we performed growth experiments by depositing a 30-monolayer-thick Ag film on an Ag(110) substrate at different temperatures and investigated the development of ordered structures by means of high resolution electron diffraction.

The experiments have been performed in an ultrahigh vacuum chamber with a base pressure of 6×10^{-11} mbar equipped with a commercial spot profile analysis–low energy electron diffraction (SPA-LEED) apparatus characterized by a transfer width of about 0.1 μm [14], a cylindrical mirror analyzer for Auger spectroscopy, and a quadrupole mass spectrometer. The Ag(110) single crystal, aligned to better than 0.2°, was cleaned by several cycles of Ne^+ ion sputtering followed by annealing up to 750 K. Ag (99.99% purity) was deposited by an electron bombardment source at a rate of 1 monolayer (ML) per minute (1 ML $= 8.45 \times 10^{14}$ atoms cm^{-2}) and the Ag film thickness was calibrated by a quartz balance. During deposition, the residual pressure in the experimental chamber was always below 1×10^{-10} mbar. Deposition was performed at different substrate temperatures, but SPA-LEED measurements were always done at 86 K. The diffraction profiles of the (00) spot were recorded for different values of the vertical scattering phase $S = K_\perp d/2\pi$ where $d = 0.144$ nm is the interlayer spacing and $K_\perp$ is the component of the electron wave vector perpendicular to the surface. Integer values of S correspond to constructive interference of waves diffracted from adjacent terraces, while half-integer values of S correspond to destructive interference, so that a maximum sensitivity to surface defects such as the steps is achieved [15]. In the following, the parallel scattering vector $K_\parallel$ will be expressed in percent units of the first Brillouin zone (% BZ) along $\langle 1\bar{1}0\rangle$.

In Fig. 1 we report the two-dimensional SPA-LEED profiles of the (00) spot obtained after deposition of 30 ML of Ag at three different temperatures. The profiles have been measured near to the $S = 2$ phase condition (constructive interference from adjacent terraces); for this scattering condition, the existence of splitted satellites indicates the presence of surface structures with a well-defined correlation length [15,16]. It clearly appears that the diffraction profiles measured after deposition at 130 and 210 K are marked by a twofold symmetry and, above all, the symmetry plane is mutually rotated by 90°, being, respectively, oriented along $\langle 1\bar{1}0\rangle$ and $\langle 100\rangle$. If we transfer this information from the reciprocal to the direct lattice we can conclude that in the experimental conditions corresponding to Figs. 1(a) and 1(c) the surface is characterized by a ripple morphology, and that a simple change of the deposition temperature from 130 to 210 K produces a 90° rotation of the ripple orientation. In particular, at 130 K the ripple ridges run along $\langle 100\rangle$, while at 210 K the ridges are parallel to $\langle 1\bar{1}0\rangle$. At the intermediate temperature of 170 K, the diffraction profile shows a pronounced fourfold symmetry [see the contour plot in Fig. 1(b)] which indicates that two characteristic correlation lengths are present along $\langle 1\bar{1}0\rangle$ and $\langle 100\rangle$, corresponding to a regular checkerboard of rectangular mounds.

In Fig. 2(a) the one-dimensional scans of the (00) spot along $\langle 1\bar{1}0\rangle$ are reported as a function of the vertical scattering phase S for the case of Ag deposition at $T = 130$ K, while in Fig. 2(b) the position of the satellite shoulders

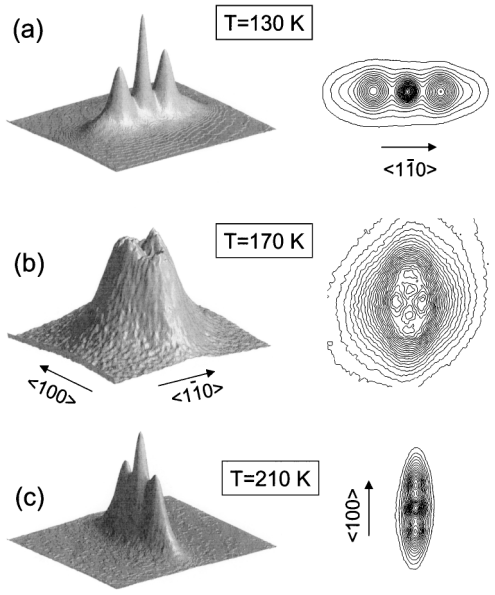

FIG. 1. Two-dimensional SPA-LEED profiles centered at the specular (00) LEED beam, measured for near in-phase diffraction conditions, after evaporation of 30 ML of Ag at a flux of 1 ML/min. The deposition temperatures are (a) 130 K, pattern size: 42% BZ, $S = 1.9$; (b) 170 K, pattern size: 27% BZ, $S = 1.84$; (c) 210 K, pattern size: 27% BZ, $S = 1.88$. Left side: 3D representations using a linear scale for the diffracted intensity. Right side: 2D contour plots of the diffracted intensity. The arrows refer to the direct space surface orientations and have a length equivalent to 10% BZ.

obtained from a Lorentzian fit is plotted versus S. It is evident that when the vertical scattering phase approaches the in-phase condition at $S = 2$, the center of the satellite peaks stagnates around q_0. The splitting $q_0 = 2\pi/\langle\Lambda\rangle$ results when the surface features are endowed with a well-defined lateral correlation length which, in the present case, is due to the average separation $\langle\Lambda\rangle$ between the ridges of the ripples [15,16]. Therefore from the measured splitting $q_0 = (6.25 \pm 0.03)\%$ BZ, we determine the ripple periodicity $\langle\Lambda\rangle_{1\bar{1}0} = 4.6 \pm 0.2$ nm. In Fig. 2(b) we can also notice that when the scattering phase S is changed towards the antiphase condition ($S = 1.5$, $S = 2.5$), two other satellites emerge which are caused by the presence of an alternating up-down staircase of steps running along the sides of the ripples. The average size of the steps $\langle\Gamma\rangle$ is obtained from the splitting of the satellites in antiphase conditions $q_1 = \pi/\langle\Gamma\rangle$ [12]. From the data of Fig. 2(b) (deposition at $T = 130$ K), by extrapolating the satellite position to the antiphase values, we find a splitting $q_1 = (33 \pm 2)\%$ BZ which corresponds to an average step size $\langle\Gamma\rangle_{1\bar{1}0} = 0.44 \pm 0.03$ nm for the majority steps which run perpendicular to $\langle 1\bar{1}0\rangle$. The same kind of analysis has been done for the experimental points recorded at higher deposition temperatures and the results are presented in Fig. 3(a). For low temperatures only the steps oriented perpendicular to $\langle 1\bar{1}0\rangle$ give a significant contribution to the diffraction signal, while for higher temperatures the steps aligned perpendicular to

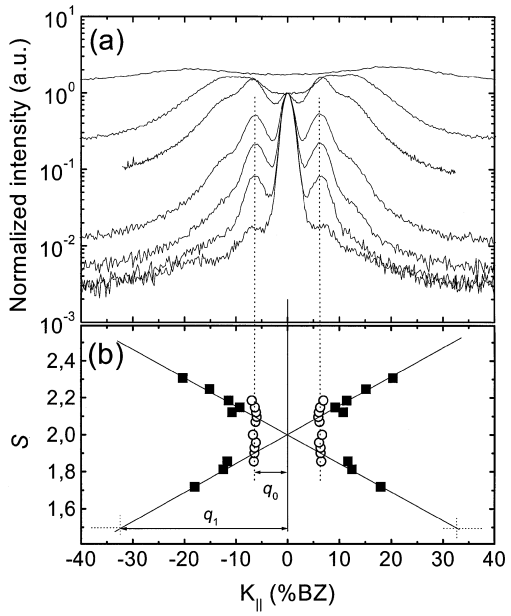

FIG. 2. Line scans of the (00) spot profile cut through $\langle 1\bar{1}0\rangle$ recorded after deposition of 30 ML of Ag at $T = 130$ K. The traces from top to bottom correspond to a vertical scattering phase $S = 1.72$, 1.81, 1.86, 1.90, 1.93, 1.96, and 2.0. All scans are normalized at the $K_{\|} = 0$ position. The top scan has been vertically offsetted. (b) Position of the satellites obtained from a Lorentzian fit is plotted vs S. Two main features can be resolved: near to the in-phase diffraction condition (hollow circles) the satellites remain centered around q_0, which indicates the presence of a well-defined lateral correlation length $\langle\Lambda\rangle_{1\bar{1}0} = 2\pi/q_0$ corresponding to the ripple wavelength. When S is shifted towards the antiphase condition, two other satellites (filled squares) emerge due to the presence of well-defined facets on the sides of the ripples. The extrapolated splitting at antiphase q_1 provides the average step size $\langle\Gamma\rangle_{1\bar{1}0} = \pi/q_1$.

$\langle 100\rangle$ (the thermodynamically favored step orientation) become dominant. In the intermediate temperature region both kinds of steps are present, again indicating that rectangular mounds are present on the surface. The average terrace length $\langle\Gamma\rangle$ defines the local surface slope m, since $m = \mathrm{atan}(d/\langle\Gamma\rangle)$, where d is the height of a monoatomic step. In the inset of Fig. 3(a) the local slope along the $\langle 1\bar{1}0\rangle$ and $\langle 100\rangle$ directions is plotted as a function of the deposition temperature. In Fig. 3(b) the ripple separation $\langle\Lambda\rangle$ along the two orientations is plotted vs deposition temperature. While the low temperature ripples, those with periodicity along $\langle 1\bar{1}0\rangle$ have $\langle\Lambda\rangle$ that grows in a limited temperature window, the high temperature ones exhibit a weaker temperature dependence.

Within the continuum model approach [10,11], the formation of moundlike structures is related to the existence of a destabilizing uphill current. In this framework, it should thus be possible to interpret our results on the anisotropic Ag(110) surface in terms of the competition between two uphill currents associated with the main surface directions, $j_{\langle 1\bar{1}0\rangle}$ and $j_{\langle 100\rangle}$. Nevertheless, the precise equation describing the currents is not straightforward because at least two assumptions of the isotropic model do not hold on an anisotropic surface: the adatoms are supposed to incorporate with equal probability at steps of different orientation, and the diffusion length l_d is considered to be isotropic. On the contrary, on the Ag(110) surface, adatoms have different incorporation rates at $\langle 1\bar{1}0\rangle$ and $\langle 100\rangle$ steps [13], while kinetic Monte Carlo simulations of submonolayer Ag growth [17] show that the island separation, and consequently also the diffusion lengths l_d, are different along $\langle 1\bar{1}0\rangle$ and $\langle 100\rangle$. Nevertheless, we emphasize that the measured local slopes of the ripple facets $m_{\langle 100\rangle}$ and $m_{\langle 1\bar{1}0\rangle}$ [Fig. 3(a)—inset] are strongly dependent on temperature and show a crossing around 160 K. Since in the isotropic case [10] the uphill current $\mathbf{j}_s(\mathbf{m})$ depends heavily on $\mathbf{m}$ [see Eq. (2)], the observed slope crossing should be reflected in a crossover of the uphill currents along the two orientations which within the continuum model should give rise to the experimentally observed ripple rotation.

A deeper insight into the evolution of the surface growth front is achieved by analyzing the elementary diffusion processes which are active during Ag deposition and their

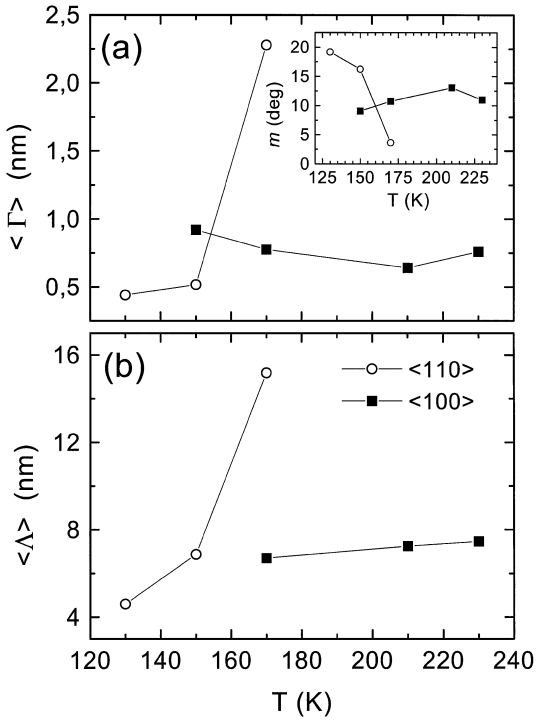

FIG. 3. (a) Average terrace size $\langle\Gamma\rangle$ along the two principal directions vs deposition temperature T. The coexistence of steps oriented perpendicular to $\langle 100\rangle$ (filled squares) and to $\langle 1\bar{1}0\rangle$ (hollow circles) in observed only in the 150–170 K temperature range where rectangular mounds are formed. For lower temperatures the majority steps are aligned perpendicular to $\langle 1\bar{1}0\rangle$, while for temperatures above 170 K the predominant step orientation is reversed by 90°. Inset: Slope m of the mounds along the two orientations. (b) Dependence of ripple wavelength $\langle\Lambda\rangle$ along the two orientations as a function of deposition temperature T. The errors resulting from the fitting procedure are comparable to the symbol size.

TABLE I. Energy barriers and activation temperatures for the elementary diffusion processes.

Elementary process	E_d (eV) [13]	Activation temperature (K) [18]
$E_{d\langle 1\bar{1}0\rangle}$	0.28	110
$E_{s\langle 1\bar{1}0\rangle}$	0.36	145
$E_{d\langle 100\rangle}$	0.38	150
$E_{s\langle 100\rangle}$	0.56	220

temperature dependence. The most important processes affecting the multilayer growth regime are adatom intralayer mass transport governed by the two energy barriers $E_{d\langle 1\bar{1}0\rangle}$ and $E_{d\langle 100\rangle}$ for diffusion along the two crystallographic directions, and adatom interlayer mass transport determined by the step edge barrier $E_{s\langle 1\bar{1}0\rangle}$ and $E_{s\langle 100\rangle}$. For the elementary diffusion process on Ag(110), following Ref. [18], it is possible to define an onset temperature T^* above which the process is considered to be activated. As results from Table I, for T well below 110 K, the activation temperature for diffusion along $\langle 1\bar{1}0\rangle$, all the relevant diffusion processes are frozen, and the surface morphology is expected to be randomly rough. For T comprised in the range 110–145 K, the temperature is high enough that adatoms can diffuse along the $\langle 1\bar{1}0\rangle$ channels but not across them and, moreover, the additional ES barrier for descent of steps oriented perpendicular to $\langle 1\bar{1}0\rangle$ cannot be overcome. This situation produces a net surface adatom flux along the $\langle 1\bar{1}0\rangle$ channels in the upward direction, i.e., what is defined as a destabilizing "uphill adatom current" responsible for the formation of periodical ripples elongated perpendicularly to the direction of the current itself [9]. This is the case of Fig. 1(a) where the ripples are observed with ridges elongated along $\langle 100\rangle$, i.e., perpendicular to the uphill current. When the deposition temperature is increased around 150 K, adatoms begin to diffuse also along $\langle 100\rangle$ and to overcome the ES barrier perpendicular to $\langle 1\bar{1}0\rangle$ steps so that a rise of the $\langle 100\rangle$ uphill current is accompanied by a reduction of the $\langle 1\bar{1}0\rangle$ one. The contemporary coexistence of these two currents explains the presence of a checkerboard of rectangular mounds observed in Fig. 1(b). If T is further increased above 150 K but still below 220 K, adatoms can diffuse along both directions, overcoming the ES barrier along $\langle 1\bar{1}0\rangle$ but not along $\langle 100\rangle$. As a consequence, the dominating uphill current becomes the one along $\langle 100\rangle$, whose effect is to produce the growth of ripples with ridges aligned along $\langle 1\bar{1}0\rangle$ as experimentally observed in Fig. 1(c). At temperatures much higher than 220 K, where both ES barriers can be surmounted, the significant interlayer mass transport is expected to reduce the surface roughness. In the present experiment we did not investigate the high temperature regime, but from the inset of Fig. 3 we notice that the slope of the ripples decreases for T above 230 K, indicating that the surface roughness begins to diminish. We notice here that a possible role for the switch of the ripple orientation at low temperatures could be played by the orientation of submonolayer islands which, as suggested by molecular dynamic simulations [17], might grow elongated along $\langle 100\rangle$ in the low temperature limit. Since at $T = 130$ K interlayer diffusion is not activated but only intralayer diffusion, the elongated submonolayer islands could thus trigger the subsequent multilayer mound growth along $\langle 100\rangle$. Further experimental work is however needed to confirm this hypothesis. The agreement between the observed surface morphologies and the hierarchy among the onset temperatures of the most relevant diffusion processes is supported by preliminary kinetic Monte Carlo simulations which show the rotation of the ripples in the expected temperature range [19].

In summary, we have shown that during multilayer homoepitaxial growth of Ag(110) a ripplelike surface instability is produced which has been quantitatively characterized as a function of deposition temperature by means of high resolution electron diffraction. Unexpectedly, as the deposition temperature is decreased from 210 to 130 K, a 90° switch of the ripple orientation has been observed. The results have been interpreted in terms of the hierarchy of inter-and intralayer diffusion barriers.

We acknowledge useful discussions with R. Ferrando and S. Rusponi.

[1] J. K. Zuo and J. F. Wendelken, Phys. Rev. Lett. **78**, 2791 (1997).
[2] J. A. Stroscio *et al.*, Phys. Rev. Lett. **75**, 4246 (1995).
[3] K. Thurmer, R. Koch, M. Weber, and K. H. Rieder, Phys. Rev. Lett. **75**, 1767 (1995).
[4] M. Bott, T. Michely, and G. Comsa, Surf. Sci. **272**, 161 (1992).
[5] G. Ehrlich and F. G. Hudda, J. Chem. Phys. **44**, 1039 (1966).
[6] R. L. Schwoebel, J. Appl. Phys. **40**, 614 (1969).
[7] C. M. Zhang *et al.*, Surf. Sci. **406**, 178 (1998).
[8] G. Amar and F. Family, Phys. Rev. B **54**, 14 742 (1996).
[9] J. Villain, J. Phys. I (France) **1**, 19 (1991).
[10] M. D. Johnson *et al.*, Phys. Rev. Lett. **72**, 116 (1994).
[11] M. Siegert and M. Plischke, Phys. Rev. Lett. **73**, 1517 (1994).
[12] M. Albrecht, H. Fritzsche, and U. Gradmann, Surf. Sci. **294**, 1 (1993).
[13] F. Hontinfinde, R. Ferrando, and A. C. Levi, Surf. Sci. **366**, 306 (1996).
[14] U. Scheithauer, G. Meyer, and M. Henzler, Surf. Sci. **178**, 441 (1986).
[15] J. Wollschlager, E. Z. Luo, and M. Henzler, Phys. Rev. B **57**, 15 541 (1998).
[16] S. Folsch, Ch. B. Choi, and K. H. Rieder, Phys. Rev. B **54**, 10 855 (1996).
[17] C. Mottet, R. Ferrando, F. Hontinfinde, and A. C. Levi, Surf. Sci. **417**, 220 (1998).
[18] K. Morgenstern, E. Laegsgaard, I. Stensgaard, and F. Besenbacher, Phys. Rev. Lett. **83**, 1613 (1999).
[19] R. Ferrando (private communication).